Dynamics and Energy Release in Fission of Small Doubly Charged Clusters

C. Brechignac, Ph. Cahuzac, F. Carlier, and M. de Frutos
Laboratoire Aime Cotton, Centre National de la Recherche Scientifique II, Campus d'Orsay, Batiment 505, 91405 Orsay Cedex, France

R. N. Barnett and Uzi Landman
School of Physics, Georgia Institute of Technology, Atlanta, Georgia 30332
(Received 12 October 1993)

Energetics and dynamics of Coulombic fission of small doubly charged potassium clusters subsequent to the ionization of singly charged ones are investigated experimentally and theoretically. Fission is shown to occur predominantly via $K_n^{++} \rightarrow K_{n-3}^{+} + K_3^{+}$ for $5 \leq n \leq 12$. The close correspondence between the measured and the calculated kinetic energy release accompanying the fission process allows a deeper understanding of the dynamics and energy redistribution mechanisms in fission of metallic clusters.

PACS numbers: 36.40.+d, 71.10.+x

Fragmentation and fission processes underlie physical and chemical phenomena in a variety of systems, characterized by a wide spectrum of energies, time scales, and nature of interactions. Recent advances in experimental and theoretical methodologies allow accurate investigations of size-evolutionary patterns of energetics and dynamics pertaining to fission phenomena in charged clusters [1,2].

Doubly charged clusters M_n^{++} are observable in mass spectra if they exceed a critical size of stability n_c^{++} [3]. For clusters with $n > n_c^{++}$ evaporation of neutral species is the preferential dissociation channel, while below this size fission into two singly charged fragments dominates [1]. Nevertheless at low enough temperature such M_n^{++} ($n < n_c^{++}$) clusters can be metastable above a certain size n_b^{++} because of the existence of a fission barrier E_b. As we show below, such a behavior develops for K_n^{++} with $n \geq n_b^{++}$ ($n_b^{++} = 7$). For cluster sizes smaller than n_b^{++} the clusters are unstable for all temperatures.

In contrast to previous experiments where only the unimolecular fission channels were observed [1] the current ones allow one to focus on small enough K_n^{++} clusters ($5 \leq n \leq 12$) where fission barriers are nonexistent (for $n < 7$) or are small (for $n \geq 7$). These first measurements of the kinetic energy release as well as the relative intensities of the different fission channels show evidence of a preferential fission channel even for hot barrierless clusters in agreement with the theoretical predictions [2].

The experimental arrangement is similar to that used in our previous work on photoinduced dissociation of K_n^{+} [4]. We use a mass-selected cluster-ion packet from a tandem time of flight. This packet interacts either with an excimer laser ($h\nu = 6.42$ eV) or a Nd YAG laser ($h\nu = 4.67$ eV) in a decelerating accelerating region. Both parents and photon induced products are spatially dispersed in the second part of the drift tube before impinging on an electron multiplier.

For a given cluster ion K_n^{+} interacting with a photon at an energy below its ionization potential only photoinduced dissociation is observed. As was shown previously [4] the laser field induces an excitation of the valence electrons which relaxes very rapidly into vibrations giving rise to sequential unimolecular dissociation. At a photon energy above the ionization threshold, two processes compete: (1) electronic excitation of K_n^{+} leading to vibrational excitation, i.e., $K_n^{+} \rightarrow (K_n^{+})^*$ and (2) ionization, $K_n^{+} \rightarrow K_n^{++} + e^{-}$. Channel (1) leads to sequential unimolecular dissociation for all cluster sizes. For small sizes channel (2) generates unstable doubly charged clusters which fission into two singly charged fragments $K_n^{++} \rightarrow K_{n-m}^{+} + K_m^{+}$.

The kinetic energy release, ϵ_r, for the Coulombic fission process induces a recoil velocity of the fragments which is measured by time dispersion in the second time of flight. Our experimental arrangement allows us to

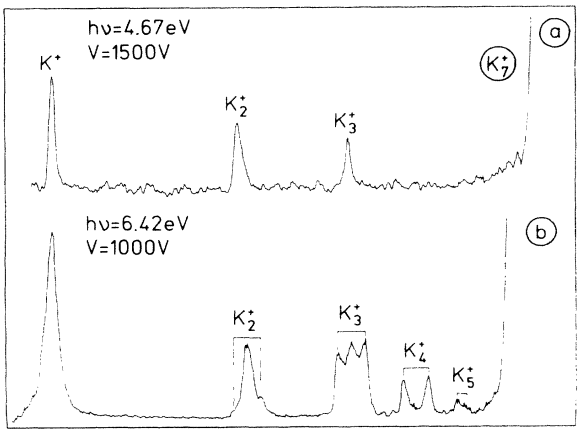

FIG. 1. Two fragmentation mass spectra of K_7^{+} after laser interaction, for photon energies below ($h\nu = 4.67$ eV) and above ($h\nu = 6.42$ eV) the ionization threshold of K_7^{+}. At $h\nu = 6.42$ eV superimposed on the evaporation pattern of hot K_7^{+} the fission channels of K_7^{++} are observed. Note that the kinetic energy release leads to a well defined splitting of the peak. The indicated voltages allow time dispersion in the time-of-flight analysis mass spectrometer; values between 800 and 1500 V were used.

0031-9007/94/72(11)/1636(4)$06.00

measure a well defined kinetic energy release, ϵ_f, of each fission fragment from the splitting of its peak in the mass spectrum. Figure 1 shows two fragmentation mass spectra of K_7^{++} for two different photon energies. It is clearly seen that the fission process of K_7^{++} leads to two observable fission channels, $K_4^+ + K_3^+$ and $K_5^+ + K_2^+$. The total ϵ_r during the fission process is given by $\epsilon_r = \epsilon_{f_1} + \epsilon_{f_2}$ with $\epsilon_{f_1}/\epsilon_{f_2} = m_{f_2}/m_{f_1}$ obeyed within 10%.

Our measurements of the total energy release ϵ_r for the observable Coulombic fission channels are given in Table I. Fission of K_{10}^{++} was not measured because K_{10}^{++} is missing in the mass spectra. The average over several series of measurements leads to an uncertainty in ϵ_r of ± 0.15 eV. We noted that among the possible fission channels for a doubly charged cluster parent, the larger the kinetic energy release, the higher the fragment peak intensity, indicating that the fission probability and kinetic energy release are connected. However, considerations of postfission evaporation processes have been included, in particular for the large clusters $n \geq 9$.

We first observe [2] that in all studied cases, even for hot barrierless K_n^{++}, the favored channel is $K_{n-3}^+ + K_3^+$ (note that K_3^+ is the first shell closing for ionized metal clusters). This behavior, which differs from the one commonly observed in nuclear physics for which hot nuclei with $3kT > E_b$ (where E_b is the fission barrier) lead to multifragmentation process [5], reflects differences between the nature of interactions, binding, and instabilities which may occur in these systems. The second best fission channel is in favor of a symmetrical (or close to) fission. This is specifically so for K_8^{++} which leads to $K_4^+ + K_4^+$ with the same energy release as the $K_3^+ + K_5^+$ channel.

Investigations of energetics, structure, and dynamics of the fission processes were performed using a method consisting of electronic structure calculations of the ground-state Born-Oppenheimer (BO) potential energy surface via self-consistent solution of the local-spin-density (LSD) functional Kohn-Sham (KS) equations (employing nonlocal pseudopotentials [6]), coupled with classical molecular dynamics (MD) of the ions (see description of the BO-LSD-MD method in [7]). Calculations using local exchange-correlation (XC) functional and XC gradient corrections (XCG) have been performed [7]. A cutoff of the plane-wave kinetic energy of 3.85 Ry was used.

Optimal configurations of the clusters (K_n, K_n^+, and K_n^{++}, $2 \leq n \leq 12$) were determined via steepest descent and dynamical simulated annealing methods. Energetics of fission channels (Δ_m^{++}, corresponding to the energy change of $K_n^{++} \rightarrow K_{n-m}^+ + K_m^+$, i.e., the energy difference between the final and the initial state) and dissociation energies (Δ_j^+ corresponding to $K_n^+ \rightarrow K_{n-j}^+ + K_j$, $j = 1,2$), calculated with XCG corrections, are given in Table I. The predominant fission channel is $K_n^{++} \rightarrow K_{n-3}^+ + K_3^+$, containing a "magic" daughter K_3^+ [2], even in cases such as $n = 10$, where a larger "magic" daughter cluster can occur (that is $K_{10}^{++} \rightarrow K_9^+ + K^+$, with K_9^+ containing an 8 electron closed shell. The theoretically calculated and experimentally measured [8] dissociation energies (Δ_1^+, Δ_2^+) are in excellent agreement. For a given cluster the most favorable experimentally observed fission channel corresponds to the final state having the lowest energy (that is lowest calculated Δ_m^{++}). Furthermore, the observed ordering between favorable fission channels and that obtained from

TABLE I. Measured and calculated energetics (in eV) for K_n^{++}. For a given n, ϵ_m corresponds to the measured kinetic energy release for the observable fission channel $K_n^{++} \rightarrow K_{n-m}^+ + K_m^+$, and the calculated (LSD-XCG) final-initial energy balance for the various channels are given by Δ_m^{++} (for simulated ϵ_3 values see Fig. 3). Calculated and experimental [8] dissociation energies are denoted by Δ_1^+ and Δ_2^+.

	n							
	5	6	7	8	9	10	11	12
ϵ_2	1.35	1.10	0.85				0.45	
ϵ_3		1.45	1.15	0.9	0.8		0.70	0.80
ϵ_4				0.9	0.75		0.40	0.40
ϵ_5							0.50	0.35
ϵ_6								0.40
$-\Delta_1^{++}$	1.27	0.97	0.87	0.83	0.675	0.51	0.49	0.16
$-\Delta_2^{++}$	1.59	1.04	1.12	0.75	0.85	0.45	0.85	0.35
$-\Delta_3^{++}$		1.57	1.41	1.21	0.97	0.85	1.01	0.92
$-\Delta_4^{++}$				0.975	0.93	0.46	0.87	0.55
$-\Delta_5^{++}$						0.63	0.72	0.66
$-\Delta_6^{++}$								0.34
Δ_1^+	0.72	0.54	0.87	0.61	0.84	0.43	0.60	0.57
Expt.	0.67	0.53	0.76	0.58	0.89	0.51	0.57	0.56
Δ_2^+	0.66	0.73	0.88	0.95	0.92	0.75	0.51	0.65
Expt.	0.60	0.69	0.77	0.83	0.94	0.89	0.55	0.61

the calculations (i.e., relative magnitudes of Δ_m^{++} for a given cluster) are in agreement.

To gain further insight, simulations of the dynamics of the fission processes have been performed. First, using constrained energy minimization (employing the local XC functional) with the center-of-mass distance $R_{\text{c.m.-c.m.}}$ between the fragments specified, fission barrier heights and shapes were determined [see E_p for K_{12}^{++} in Fig. 2(a)]. For the energetically favorable channel (i.e., $K_{n-3}^{+}+K_3^{+}$) fission barriers ($E_b^{(3)}$) exist for $n>6$ and their magnitudes are 0.08, 0.14, 0.31, 0.495, 0.25, and 0.2 eV for $n=7$ to $n=12$, respectively. We note the high barrier for fission of K_{10}^{++} reflecting the $8e^-$ closed shell ("magic number") structure of the cluster. The barriers for other fission channels are of larger magnitudes than those corresponding to the $m=3$ channel; e.g., the barriers, $E_b^{(1)}$ for fission leading to $K_{n-1}^{+}+K^{+}$ for $n=7$ and 8 are 0.38 and 0.31 eV, respectively.

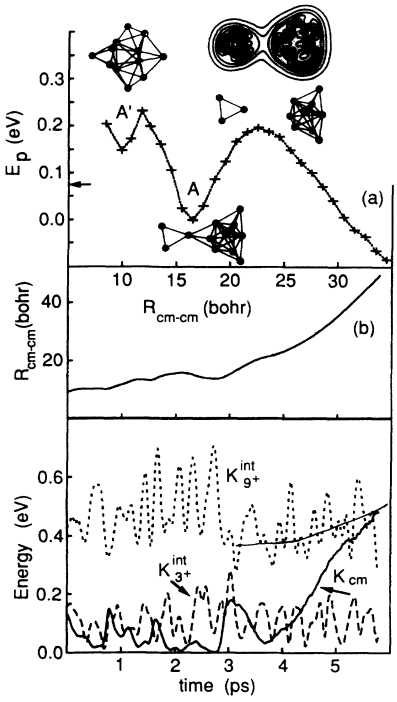

FIG. 2. (a) Potential energy (E_p) of K_{12}^{++} versus $R_{\text{c.m.-c.m.}}$ obtained via constrained minimization. The origin of the E_p scale is set at the optimal prebarrier configuration (A). For large $R_{\text{c.m.-c.m.}}$, $E_p=-0.9$ eV, i.e., Δ_3^{++}. Included also are cluster configurations of K_{12}^{++} corresponding to a compact isomer (A') (the energy of the optimal compact isomer found is denoted by an arrow), the optimal bound configuration (A), and the structure on top of the exit-channel barrier for which contours of the total electronic charge density, ρ, are shown. (b) Time evolution of $R_{\text{c.m.-c.m.}}$, the internal vibrational kinetic energies of the fragments (K_3^{int} and K_9^{int}) and the sum of the fragments' translational kinetic energies ($K_{\text{c.m.}}$) obtained via a BO-LSD-MD simulation starting from ionization ($t=0$) of a K_{12}^{+} cluster at 500 K. A line is drawn in K_9^{int} (for $t\geq 3$ ps) to guide the eye.

Of particular interest are the barrier shapes along the fission coordinate ($R_{\text{c.m.-c.m.}}$), exhibiting double (or multiple) humps [see Fig. 2(a)]. Underlying such barrier shapes, discussed earlier in the context of nuclear fission [9] and more recently for metal clusters [2], are lifting of degeneracies of the electronic energy levels due to the structural deformations and shape distortions accompanying the fission process [2,9].

To address issues pertaining to dynamics of the fission process, we have performed BO-LSD-MD simulations (using the local XC functional) starting (for each size) from few configurations of a K_n^{+} cluster equilibrated at the desired temperature (simulations for both $T=250$ and 500 K were performed). Given a selected state of K_n^{+} an electron occupying the highest occupied KS orbital was removed (corresponding to ionization) and the resulting K_n^{++} cluster was allowed to evolve until the distance between the fission fragments was large enough ($R_{\text{c.m.-c.m.}}\geq 50$ a.u.) so that the residual interfragment interaction can be attributed solely to electrostatic Coulomb repulsion. We note that in all simulations where the initial K_n^{+} was ionized to yield a low-spin configuration of the K_n^{++} cluster fission into the energetically favorable channel ($p=3$) occurred for all sizes [10]. Results are shown in Fig. 2(b) for the fission of $K_{12}^{++}\rightarrow K_9^{+}+K_3^{+}$, starting from K_{12}^{+} at 500 K, in correspondence with the experimental conditions [8].

The case of K_{12}^{++} is particularly interesting since the energetically favorable fission channel consists of two magic number daughters (K_9^{+} and K_3^{+}). As seen from Fig. 2(a) the lowest energy local-minimum structure of K_{12}^{++} is highly deformed with the eventual fission products recognized already in the prebarrier stage (A). This highly deformed state is separated by a barrier from higher-energy isomers (A') which possess compact structures close to that of the K_{12}^{+} cluster. In contrast, all other K_n^{++} clusters ($6<n<12$) are characterized by compact structures of the optimal prebarrier states. For these clusters higher-energy deformed bound-state isomers are located "on top" of the barrier (as local minima) separated from the exit channel by a potential energy "hump" [2].

The dynamical evolution of the system is shown in Fig. 2(b). The system starts from a high-energy compact isomer of K_{12}^{++} reached by the ionization event and its evolution toward the optimal distorted structure [local minimum A in Fig. 2(a)] for $t\leq 3$ ps is accompanied by a gradual increase in $R_{\text{c.m.-c.m.}}$, a decrease in the potential energy of the system, vibrational cooling of the cluster (most noticeable in K_9^{int}), and transfer of energy into the interfragment degree of freedom ($K_{\text{c.m.}}$). Climbing the potential barrier leading to separation of the fission products [$3\leq t\leq 3.7$ ps, in Fig. 2(b)] is accompanied by cooling of the interfragment translational motion ($K_{\text{c.m.}}$). Subsequent separation of the fragments [see $R_{\text{c.m.-c.m.}}$ in Fig. 2(b) for $t\geq 3.7$ ps] in the exit channel accelerates the fragments' motion as portrayed by a steep increase of

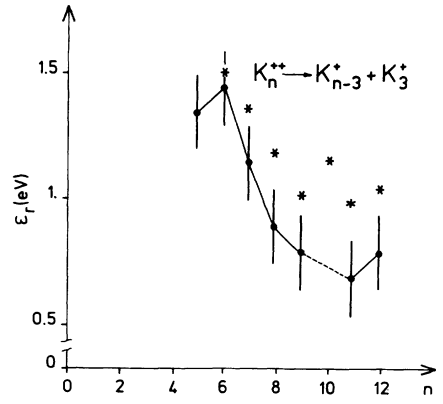

FIG. 3. Kinetic energy release, ϵ_r, for $K_n^{++} \rightarrow K_{n-3}^{+} + K_3^{+}$. Experimental values are shown with vertical error bars and results obtained via dynamical simulations are denoted by *. For the "magic" K_{10}^{++} cluster only the calculated ϵ_r is shown.

$K_{\text{c.m.}}$ (in the limit of large separation $\epsilon_r = K_{\text{c.m.}}$). During the separation process the kinetic energies of the internal degrees of freedom of the fragments increase, resulting in vibrational heating of the fission products in the exit channel (see in particular K_9^{int}). Consequently, the fission products emerge vibrationally hot, which correlates with experimentally observed postfission evaporation events. In such cases, for K_n^{++} with $n = 9, 11, 12$, odd-even alternation is observed in the measured fragmentation pattern. Hence except for the most asymmetrical fission channel $K_3^{+} + K_{n-3}^{+}$ the kinetic energy release is measured less accurately.

The experimentally determined values and those obtained from dynamical simulations of the kinetic energy release in the channel $K_n^{++} \rightarrow K_{n-3}^{+} + K_3^{+}$ for $5 \leq n \leq 12$ shown in Fig. 3 are in close correspondence. We remark that for K_n^{++} clusters with $n \leq 8$ the kinetic energy release values obtained in simulations with $T = 250$ K of the initial K_n^{+} clusters were lower than those determined for $T = 500$ K.

In a dynamical simulation, once the fragments are distinguishable (prebarrier or on top of the fission barrier), the finite-temperature total energy can be expressed as $E_{\text{tot}}(t) = E_p(R_{\text{c.m.-c.m.}}(t)) + K_{\text{c.m.}}(t) + \epsilon(t)$, where E_p is the $T = 0$ energy corresponding to optimal configurations determined for interfragment separations $R_{\text{c.m.-c.m.}}$ [see Fig. 2(a)] and $\epsilon(t) = \delta\epsilon_p(t) + K^{\text{int}}(t)$ is the sum of the finite-temperature potential and internal kinetic energy contributions. We observed that on top of the exit barrier $(t = t_b)\, \delta\epsilon_p(t_b) > K^{\text{int}}(t_b)$; additionally after separation $(t = t_\infty)$ we found that $K_{\text{c.m.}}(t_\infty) \equiv \epsilon_r \simeq -\Delta_3^{++} + E_b$ (see Fig. 3 [11]), and $K_{\text{c.m.}}(t_\infty) \gg K_{\text{c.m.}}(t_b)$. Moreover, from our simulations $K^{\text{int}}(t_\infty) > K^{\text{int}}(t_b)$ which, together with the above observations, leads us to conclude that the observed heating of the products in the exit channel originates from dynamical redistribution of ϵ, i.e., conversion of the excess potential $[\delta\epsilon_p(t_b) > \delta\epsilon_p(t_\infty)]$ into internal energy rather than into the release kinetic energy $K_{\text{c.m.}}$.

Finally, these investigations suggest further studies including spectroscopy of long-lived metastable fission isomers (we note that in our simulations of the larger clusters $n > 8$ for $T = 250$ K fission times up to 10^2 ps were observed) and effects due to spin states [10].

The work of R.N.B. and U.L. was supported by the U.S. Department of Energy, Grant No. FG05-86ER-45234. Calculations were performed at the Florida State University Supercomputer Center.

[1] C. Brechignac *et al.*, Phys. Rev. Lett. **64**, 2893 (1990).
[2] R. N. Barnett, U. Landman, and G. Rajagopal, Phys. Rev. Lett. **67**, 3058 (1991), and references therein; R. N. Barnett and U. Landman, *ibid.* **69**, 1472 (1992).
[3] K. Sattler *et al.*, Phys. Rev. Lett. **47**, 160 (1981).
[4] C. Brechignac *et al.*, Phys. Rev. Lett. **63**, 1368 (1989).
[5] W. Lynch, Annu. Rev. Nucl. Part. Sci. **37**, 493 (1987); D. H. E. Gross, Rep. Prog. Phys. **53**, 605 (1990); D. R. Bowman *et al.*, Phys. Rev. Lett. **67**, 1527 (1991).
[6] N. Troullier and J. L. Martins, Phys. Rev. B **43**, 1993 (1991).
[7] R. N. Barnett and U. Landman, Phys. Rev. B **48**, 2081 (1993).
[8] C. Brechignac *et al.*, J. Chem. Phys. **10**, 7449 (1990).
[9] M. A. Preston and R. Bhaduri, *Structure of the Nucleus* (Addison-Wesley, Reading, MA, 1975), p. 589; For a discussion of electronic shell effects on cluster-fission barriers see C. Yannouleas, R. N. Barnett, and U. Landman, Commun. At. Mol. Phys. (to be published).
[10] We observed in our simulations that by starting from a high-spin configuration of a K_n^{++} cluster one can preclude energetically the $m = 3$ channel, resulting in fission into another channel. For example, starting from $K^{++}(4\uparrow, 2\downarrow)$, i.e., $S = 1$ spin state, leads to fission into $2K_4^{+}(2\uparrow, \downarrow)$ (involving a barrier of 0.12 eV), rather than $K_5^{+}(3\uparrow, 1\downarrow) + K_3^{+}(\uparrow, \downarrow)$. We also calculated (using LSD-XCG) that the ionization potential of K_8^{+} to yield the $S = 1$ state of K_8^{++} is only 0.18 eV higher than that leading to the $S = 0$ state. The occurrence of such processes may correlate with the relatively high probability with which the symmetric fission channel ($2K_4^{+}$) was experimentally observed.
[11] Since in the simulations LSD was used (without XCG corrections), for direct comparison with the results for ϵ_r given in Fig. 3 use the E_b values given in the text with $-\Delta_3^{++} = 1.5$, 1.28, 1.04, 0.79, 0.67, 0.85, and 0.86 eV for $n = 6$ to $n = 12$, respectively.